


# The explosive-effusive transition within the Miocene Fataga suite, Gran Canaria

**Journal Article****Author(s):**

Baumann, N.B.; Ellis, Ben; Cortes-Calderon, Edgar A.; [Szymanowski, Dawid](#) ; Harris, Chris; Bachmann, Olivier

**Publication date:**

2023-01-20

**Permanent link:**

<https://doi.org/10.3929/ethz-b-000588375>

**Rights / license:**

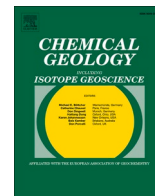
[Creative Commons Attribution 4.0 International](#)

**Originally published in:**

Chemical Geology 616, <https://doi.org/10.1016/j.chemgeo.2022.121242>

**Funding acknowledgement:**

197040 - Defining 'super-eruptive' frequencies from the Yellowstone hotspot track (SNF)



## The explosive-effusive transition within the Miocene Fataga suite, Gran Canaria

N.B. Baumann<sup>a,b</sup>, B.S. Ellis<sup>a,\*</sup>, E.A. Cortes-Calderon<sup>a</sup>, D. Szymanowski<sup>a,c</sup>, C. Harris<sup>d</sup>, O. Bachmann<sup>a</sup>

<sup>a</sup> Institute of Geochemistry and Petrology, ETH Zurich, Clausiusstrasse 25, 8092 Zurich, Switzerland

<sup>b</sup> Friedrich-Alexander-Universität Erlangen-Nürnberg, GeoZentrum Nordbayern, Schlossgarten 5, 91054 Erlangen, Germany

<sup>c</sup> Department of Geosciences, Princeton University, Guyot Hall, Princeton, NJ 08544, USA

<sup>d</sup> Department of Geological Sciences, University of Cape Town, Rondebosch 7700, South Africa

### ARTICLE INFO

Editor: Claudia Romano

#### Keywords:

Explosive-effusive transition

Gran Canaria

Megacryst

Oxygen isotopes

Pb isotopes

### ABSTRACT

Many volcanoes show transitions between explosive and effusive eruptive styles both through the history of the volcano as a whole and occasionally within the course of a single eruption. These differing eruptive styles have vastly different implications for hazard assessments in surrounding regions and so understanding such changes is important. Here, we investigate the intercalated lavas and ignimbrites of the Miocene Fataga Group on the island of Gran Canaria, Spain. Ignimbrites reflect the products of explosive events from the Tejedá caldera, while lavas found within the pyroclastic succession were erupted from extra-caldera sources some 5–10 km from the caldera margin. The ignimbrites exhibit textural complexity containing both crystal-poor juvenile pyroclasts and late-erupted crystal-rich juvenile clasts interpreted to reflect interaction between cumulates and recharge magmas. The lavas meanwhile are almost phenocryst-free, with the exception of few large (cm-scale), unzoned sanidine crystals. Despite their textural differences, the lavas are geochemically similar (in terms of bulk rock and feldspar compositions) to the crystal-poor juveniles in the ignimbrites. Oxygen and lead isotopic compositions of the lavas and surrounding ignimbrites reveal that the magmas shared a deeper source and that petrographic variability is imprinted upon the magmas at shallow levels. We interpret the lavas as originating from peripheral magmatic pockets, on the edges of the main caldera-feeding reservoir. These peripheral magma chambers felt the effects of recharge only as slight thermal fluctuations that fostered the production of the large sanidine crystals. Our findings highlight the potential for storage of magmas aside from the main magmatic system that may represent an underappreciated hazard at volcanoes worldwide.

### 1. Introduction

Volcanoes from all tectonic settings exhibit transitions in styles of eruptive behaviour between explosive and effusive and vice versa (Di Genova et al., 2017; Cassidy et al., 2018; Popa et al., 2019). This ‘explosive-effusive transition’, as it is commonly termed, represents a challenge for volcanology as the hazards associated with these eruptive styles are significantly different. Transitioning between explosivity and effusivity may happen in sequential eruptions throughout the history of the volcano (Christiansen, 2001; Popa et al., 2019) or within a single eruption (Adams et al., 2006; Schipper et al., 2013), with transitions in either direction reported. In many cases, the magmas that gave rise to these explosive and effusive eruptions exhibit only subtle variations in

their compositions and their inferred storage conditions (Di Genova et al., 2017) and so the driving force that produces this different behaviour often remains elusive. Some studies have inferred that changes occurring in the magmatic reservoir play a major role (e.g., Popa et al., 2021) while others have proposed a dominant role for processes occurring on a smaller spatial scale within the conduit (e.g., Tuffen et al., 2003; Wadsworth et al., 2020), particularly where eruptive style transitions during a single eruptive event (Cassidy et al., 2018).

In this study, we focus on a case where the explosive and effusive products of a single volcano have drastically different petrographic properties (e.g., crystallinity, mineral assemblages). The Miocene Fataga succession of Gran Canaria (Canary Islands, Spain) shows lavas erupted from sources on the flanks of the edifice intercalated with ignimbrites

\* Corresponding author at: Institute of Geochemistry and Petrology, ETH Zurich, Clausiusstrasse 25, 8092 Zurich, Switzerland.

E-mail address: [ben.ellis@erdw.ethz.ch](mailto:ben.ellis@erdw.ethz.ch) (B.S. Ellis).

<https://doi.org/10.1016/j.chemgeo.2022.121242>

Received 7 October 2022; Received in revised form 17 November 2022; Accepted 27 November 2022

Available online 1 December 2022

0009-2541/© 2022 The Authors. Published by Elsevier B.V. This is an open access article under the CC BY license (<http://creativecommons.org/licenses/by/4.0/>).

erupted from the centre of the volcano (forming calderas). While [Cortes-Calderon et al. \(2022\)](#) provided an in-depth study of the pyroclastic units, we here investigate the effusive deposits that are temporally close (available  $^{40}\text{Ar}/^{39}\text{Ar}$  geochronology of ignimbrites bracketing the lavas are only separated by tens of thousands of years, [Cortes-Calderon et al., 2022](#)). While the explosive deposits are petrographically variable, their effusive counterparts are homogenous. Shedding light on the petrogenesis of the Fataga lavas will not only help to expand the understanding of Gran Canaria's magmatic evolution but potentially provide critical insight into the controls of explosive-effusive transitions and thus help to improve volcanic hazard assessment for the Canary Islands and other volcanic regions.

## 2. Geological background

The volcanic archipelago of the Canary Islands lies atop thick Jurassic ocean crust off the northwestern coast of Africa ([Fig. 1](#)) and is widely acknowledged to be the result of a mantle upwelling or 'hotspot' ([Wilson, 1963; Montelli et al., 2006](#)). Gran Canaria, situated in the centre of the island group, has a volcanic history known to extend for at least 14.3 myr ([McDougall and Schmincke, 1976](#)). Gran Canaria is placed third in the relative island age progression of Fuerteventura being the oldest, followed by Lanzarote, Gran Canaria, La Gomera, Tenerife, Hierro and finally La Palma ([Abdel-Monem et al., 1971, 1972](#)). The ongoing volcanic activity in the Canary Islands was recently highlighted by the eruption at the Cumbre Vieja volcanic ridge, La Palma in 2021.

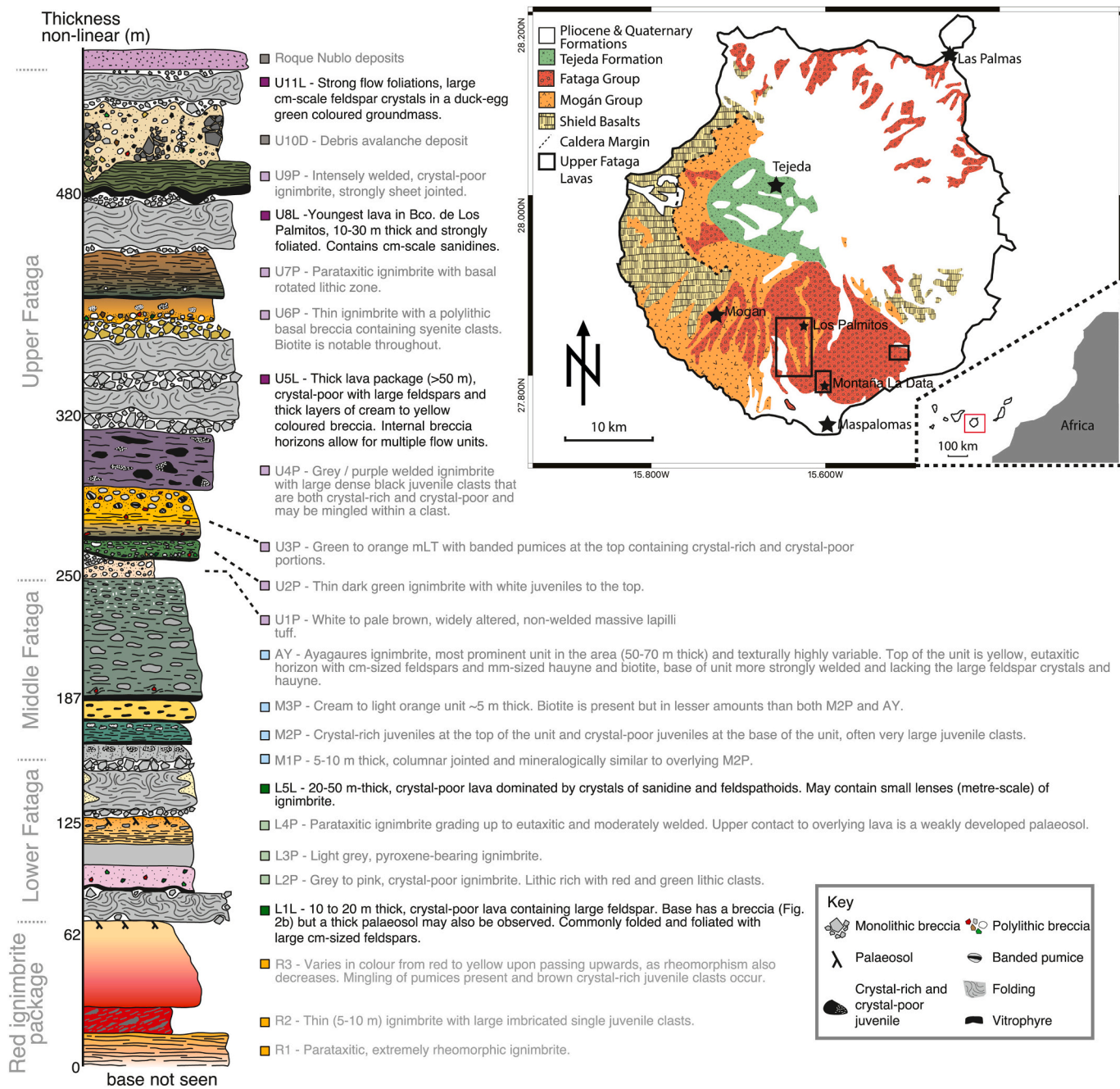


**Fig. 1.** Geological background of the Fataga lavas (modified after [Cousens et al., 1990; Schmincke, 1976; Balcells-Herrera et al., 1992](#)). Main map shows the location of sample areas from this study. Inset shows the location of the Canary Islands. Generalised vertical succession (GVS) shows the stratigraphy of the Fataga deposits in the study area (modified after [Cortes-Calderon et al., 2022](#)).

The first stage of subaerial volcanism on Gran Canaria is reflected by the presence of shield basalts (McDougall and Schmincke, 1976). Almost immediately following the cessation of the basaltic shield building stage (Van den Bogaard and Schmincke, 1998), explosive silicic (rhyolitic) volcanism occurred at ~14 Ma producing the distinctively zoned P1 ignimbrite (Freundt and Schmincke, 1992). Once established, explosive silicic volcanism continued from the Tejeda caldera for some five million years (Van den Bogaard and Schmincke, 1998). The first erupted materials, the Mogán Group, represent silica-oversaturated magmas that were predominantly erupted in explosive events. The Mogán suite of rocks also contains mafic lavas (hawaiite, mugearite, e.g., units T3, T6; Sumita and Schmincke, 1998). Over time, magmas transitioned to silica-undersaturated compositions that characterise the Fataga Group. The record of effusive volcanism in the Fataga Group remains incompletely known, but it appears to encompass only evolved compositions and the proportion of effusive volcanism appears to increase with time (more lavas in the upper parts of the stratigraphic sections; Balcells-Herrera et al., 1992; Carracedo and Troll, 2016; Cortes-Calderon et al., 2022). Following the cessation of Miocene volcanism, an eruptive hiatus of more than two million years occurred prior to a rejuvenation marked by the Roque Nublo and post-Roque Nublo activity (Pérez-Torrado et al., 1995; Hoernle and Carracedo, 2009). The most recent eruptive activity on Gran Canaria, the Bandama explosive event, occurred approximately two thousand years ago (Rodríguez-González et al., 2009).

### 2.1. The Fataga group

The transition between Mogán and Fataga volcanism and the overall stratigraphy of much of the Miocene volcanism on Gran Canaria remains poorly constrained. Sumita and Schmincke (1998) refer to ‘about six’ oxidised, red ignimbrites in the Montana Horno Formation that have a mineralogy similar to overlying Fataga units (e.g., containing abundant biotite, which is subordinate in Mogán deposits) while having bulk rock compositions more akin to the underlying Mogán units. Van den

Bogaard and Schmincke (1998) place these deposits as erupted between  $13.50 \pm 0.08$  Ma and  $13.25 \pm 0.08$  Ma with the first unit they unequivocally denote as Fataga dated to  $12.63 \pm 0.07$  Ma ( $^{40}\text{Ar}/^{39}\text{Ar}$  ages recalculated to the Fish Canyon sanidine standard at 28.294 Ma, Renne et al., 2011). In the newest work on the Fataga volcanism, Cortes-Calderon et al. (2022) define the first Fataga unit within their stratigraphy in the Barranco de La Data as a lava (L1L) which overlies a red ignimbrite dated to  $13.826 \pm 0.036$  Ma and underlies their L4P unit dated to  $13.355 \pm 0.027$  Ma. Cortes-Calderon et al. (2022) designated the units in their study area with three-digit codes, the first referring to the relative stratigraphic position – lower, middle, or upper (L, M, or U), the second referring to the number of the unit within that group (1–11) and a final L (lava) or P (pyroclastic) indicator. Here we follow this stratigraphy as it is the most complete record of Fataga volcanism (Fig. 1).

## 3. Methods

### 3.1. Samples and sample characterisation

Samples of lavas from the Fataga succession were taken following the new stratigraphy of Cortes-Calderon et al. (2022) predominantly in the barrancos of Los Palmitos and Chamoriscan and in vicinity of Montaña la Data (Figs. 1 and 2). Ignimbrite samples were provided by previous fieldwork (i.e., Cortes-Calderon et al., 2022). The lavas range in thickness from a few metres to up to fifty metres and typically exhibit large folds in their upper reaches. In some cases (L1L, U5L), they are internally complex with lenses of pyroclastic material within or with medial breccias suggesting multiple flow units may exist. Petrographically, they are monotonous, microcrystalline and have low phenocryst abundance. Where phenocrysts do occur, they are typically cm-scale and are readily distinguished from the grey groundmass due to their highly reflective, fresh, appearance. On the other hand, ignimbrites display an immense textural and structural variety in the Fataga Group. Especially the grade of welding, single juvenile clast content, crystallinity and overall

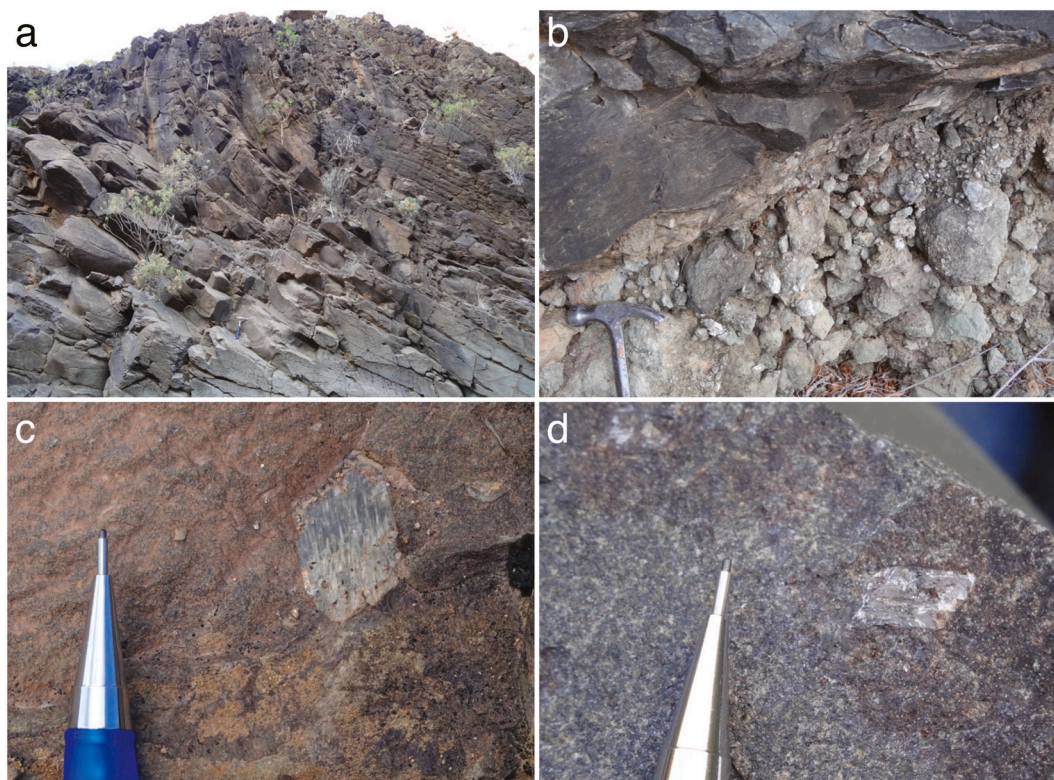


**Fig. 2.** Appearance of the Fataga lavas in the field. A. Large scale folds in the upper surface of U5L unit, Barranco Chamoriscan, field of view approximately 5 m. B. Breccia at the base of the L1L unit, Barranco La Data C. Centimetre-scale crystals in the U8L unit D. Centimetre-scale crystals in the U5L unit.

mineral assemblage differ strongly between different pyroclastic units (Fig. 1). To quantify the petrographic differences observed in the field, we carried out point counting analyses of thin sections from ignimbrites and lavas of the Fataga suite. Crystals above 250  $\mu\text{m}$  in longest dimension were considered as phenocrysts and their areal abundance on the thin section was measured. In the ignimbrites, we focussed on the proportion of crystals occurring within fiammé to define crystal content of the magma prior to eruption and so be most directly comparable to the lavas. In a few ignimbrites, we additionally measured the phenocryst content of the whole thin sections to observe the relative difference between bulk and juvenile components.

### 3.2. Bulk rock compositions

Bulk rock samples (~30 g) for XRF and ICP analyses were prepared following standard procedures at ETH Zurich (Troch et al., 2018). Subsequent analyses were carried out using a PANalytical Axios WD-XRF spectrometer. LA-ICP-MS analyses were carried out using an Excimer 193 nm (ArF) GeoLas (Coherent) laser system coupled to a Perkin Elmer Nexion2000 fast-scanning quadrupole ICP-MS at ETH Zurich. The primary standard was NIST SRM610 (Jochum et al., 2011) glass and the secondary reference material USGS BCR-2 (Raczek et al., 2001). For the subsequent data-reduction SILLS, a MATLAB-based program (Guillong et al., 2008) was used.  $\text{SiO}_2$  concentrations of prior XRF results were used as internal standards for the ICP-MS measurements. All data and detailed analytical procedures for this study are provided in supplementary materials.

### 3.3. Mineral texture and chemistry

With the low number of phenocrysts per volume of rock found in the lavas, we employed a targeted approach to crystal analysis. Single feldspar crystals were mounted in epoxy and polished using sandpaper first and diamond paste afterward, gradually decreasing grain size down to 1  $\mu\text{m}$ . The crystal mounts were analysed using a JEOL JSM-6390 LA scanning electron microscope (SEM) and a Deben Centaurus panchromatic cathodoluminescence detector at ETH Zurich to obtain both back-scattered electron (BSE) and cathodoluminescence (CL) images and thus identify feldspar zonation.

In-situ analytical work on the feldspar crystals was guided by the textures observed in BSE images. Major elemental compositions of sanidine crystals were measured using JEOL JXA-8200 and JEOL JXA 8230 Electron Probe Microanalysers (EPMA), both equipped with five wavelength dispersive spectrometers (WDS), hosted at the Institute of Geochemistry and Petrology at ETH Zurich. The EPMA was operated at 15 kV with a beam diameter of 10  $\mu\text{m}$  and a probe current of 20 nA. On-peak counting times for all elements was 30 s, mean atomic number (MAN) background intensity fits were used to calibrate the background and continuum absorption corrected for all elements (Donovan and Tingle, 1996; Donovan et al., 2016). Na and K were analysed first to minimise alkali migration and time dependent intensity (TDI) was employed to restore original values when required. The primary standards used were rutile for titanium (Ti), strontianite for strontium (Sr), barite for barium (Ba), albite for sodium (Na) and silicon (Si), forsterite for magnesium (Mg), anorthite for aluminium (Al) and calcium (Ca), fayalite for iron (Fe), microcline for potassium (K). Unknown and standards intensities were corrected for deadtime. Reference materials were run together with the unknowns in a sample-standard bracketing manner. Primary standard intensities were corrected for drift over time. The matrix correction method was PRZ algorithm (Goldstein et al., 1981). The calculations and mass absorption coefficients dataset was FFAST Chantler (NIST v 2.1, 2005). The Probe for EPMA software (Donovan et al., 2018) was used to collect and process the data. Trace elemental compositions of the sanidines were measured using a 193 nm Resonetics (ArF) excimer laser coupled with a Thermo Element XR LA-ICP-MS located in the institute of Geochemistry and Petrology, ETH

Zurich, with analysis and subsequent data reduction as described by Szymanowski et al. (2015). For data reduction the typical  $\text{SiO}_2$  content of the sanidines (65.71%) was used as internal standard based on the data obtained by EPMA. All new results and secondary standard data are provided in supplementary materials.

Qualitative WDS element maps of feldspar megacrysts were acquired with a JEOL JXA 8230 EPMA at ETH Zürich. The EPMA was operated at 15 kV with a probe current of 80 nA and a beam diameter of 10  $\mu\text{m}$ . Pixel size was set to 10  $\mu\text{m} \times 10 \mu\text{m}$  and dwell time to 80 ms. Five elements (Si, Ca, K, Fe, Na) were mapped simultaneously in individual spectrometers. Peak positions, bias and base line windows were acquired by measuring primary standards such as albite (Si and Na), anorthite (Ca), microcline (K) and fayalite (Fe).

### 3.4. Oxygen isotopes

Oxygen isotopic compositions were determined from feldspar crystals that were separated from crushed lava under a binocular microscope and cleaned in.

dilute nitric acid and deionised water. The measurements were made at the Department of Geological Sciences, University of Cape Town, South Africa, via laser fluorination using a 20 W NewWave  $\text{CO}_2$  laser following methods described in Harris and Vogeli (2010) except with 20 kPa  $\text{ClF}_3$  as reagent. Sample sizes were typically on the order of a few mg and comprised a few of the large feldspar crystals. A Finnegan DeltaXP mass spectrometer in dual inlet mode was used to analyse isotope ratios offline. Results are presented relative to SMOW (standard mean ocean water) with  $\delta = [({}^{18}\text{O}/{}^{16}\text{O})_{\text{sample}} / ({}^{18}\text{O}/{}^{16}\text{O})_{\text{SMOW}} - 1] * 1000$ . The composition of the Monastery garnet (MON GT  $\delta^{18}\text{O} = 5.38 \text{‰}$ , Harris and Vogeli, 2010) standard was used to normalise unknowns. The multi-year average range of MON GT duplicates via laser fluorination (2 per session) is 0.12‰ (based on 393 pairs), with a  $2\sigma$  value of 0.16‰. Alkali feldspar yields were systematically low (27 to 85%, avg. 66%) but there is no correlation between yield and  $\delta^{18}\text{O}$  value ( $r = -0.19$ ). We, therefore, consider the  $\delta^{18}\text{O}$  values obtained to be robust.

### 3.5. Pb isotopes

For radiogenic isotopes we focus on Pb given the unreliability of Sr (Cousens et al., 1993) and the larger dataset of Pb in the literature. Pb isotopes were analysed at Princeton University in sanidine separates consisting of 5–20 inclusion-free, millimetre-sized crystal fragments. The selected crystals were leached at 120 °C in 6 M HCl + 15 M  $\text{HNO}_3$  for 2 days, repeatedly rinsed with deionised water and dissolved in double-distilled 29 M HF (1.4 ml) + 15 M  $\text{HNO}_3$  (0.6 ml) at 150 °C for 3 days. Lead was separated using anion exchange chromatography on 100  $\mu\text{l}$  columns in 0.5 M HBr medium. Total procedural blanks were < 1 pg Pb which is considered negligible for the unknowns which contained ng levels of Pb. The samples were loaded in silica gel on single degassed Re-filaments and analysed using an Isotopx Phoenix thermal ionisation mass spectrometer equipped with ATONA amplifiers (Szymanowski and Schoene, 2020) using static Faraday cup collection. Instrumental mass fractionation was corrected with a factor of  $0.089 \pm 0.042\text{‰/amu}$  ( $2\sigma$ ) based on compiled measurements of NIST SRM 982 and of double-spiked Pb isotope analyses. The uncertainty on the instrumental mass fractionation factor was fully propagated into final uncertainties.

## 4. Results

### 4.1. Componentry

As in the ignimbrites, feldspar is the dominant mineral phase in the lavas. Yet, this one similarity aside, the lavas and ignimbrites have distinctly different petrography. In terms of overall crystallinity (here referring to crystals with a long axis > 250  $\mu\text{m}$  rather than groundmass crystallinity), the lavas range from 0.2 to 1.0% while the ignimbrites

range from 4.7 to 16.0% in bulk samples and 3.2–6.5% (Fig. 3) when only considering the crystallinity of the fiammé. The fiammé are likely the better comparison with the lavas given that they most closely reflect the state of the magma and are less affected by post-eruptive processes of ash winnowing and crystal concentration than bulk ignimbrite. In the lavas, mafic phases are not observable in hand specimen while they are common in the ignimbrites. Exceptionally large feldspar phenocrysts up to 2 cm in length are only found in the lavas.

#### 4.2. Bulk rock compositions

Individual juvenile clasts from the Fataga succession are trachytic in bulk composition with juveniles from the lowermost part of the stratigraphy of Cortes-Calderon et al. (2022) extending to the highest SiO<sub>2</sub> contents. A number of the Fataga ignimbrites contain crystal-rich juveniles in addition to the ubiquitous crystal-poor juveniles. These crystal-rich clasts are also trachytic in bulk compositions but show distinctive trace element signatures with elevated Ba contents and Eu/Eu\* (Fig. 4). The lavas, despite their starkly different appearance, have bulk compositions that approximate those of the crystal-poor juveniles at a given stratigraphic interval albeit offset to more phonolitic / silica-undersaturated compositions (Fig. 4). The crystal-poor lavas from the Upper Fataga are the only samples that are phonolitic in bulk composition.

#### 4.3. Mineral textures and compositions

Texturally, the large crystals within the lavas are relatively simple. They contain few, if any, inclusions of other phases or melt and show very little chemical zoning. Some slight zonation can be seen in cathodoluminescence imaging, but is much subdued compared to the variability observed within feldspars from the surrounding ignimbrites with examples of these strongly zoned feldspars found in the ignimbrites shown in Fig. 5. Similarly, semi-quantitative compositional maps of the large feldspar crystals in the lavas exhibit limited zonation (Sup. Fig. 1).

Compositionally, all the large feldspar crystals within the lavas are sanidine (Fig. 6). The 538 new measurements of feldspars (both large crystals and groundmass) in this study show an overall range in

KAlSi<sub>3</sub>O<sub>8</sub> content (henceforth referred to as “Or”) of 28 to 46%mol with an average of Or 38 ± 5%mol (Fig. 6). The lowest Or contents are found in L1L (28 to 37%mol, avg. Or 32 ± 4%mol) while the overlying lavas range from Or contents of 31 to 46%mol and have an overall average of Or 39 ± 3%mol. Notably, the lavas show much less compositional variability than the ignimbrites, which span a range of Or 6.8 to 41.7% mol with an average of Or 34 ± 10%mol (Fig. 7). In the cases where groundmass phases were measured in addition to the megacrysts (L1L, U11L), the groundmass feldspars are not different in composition, supportive of the large crystals being broadly in equilibrium with their carrier melt. In the lava samples from the upper Fataga, small crystals of nepheline also occur.

In terms of trace elements, single large sanidine crystals show limited variation both within a crystal and between crystals (Figs. 5, 7). The stratigraphically lowest unit studied here, L1L, has trace elemental compositions that are somewhat distinct from the overlying lavas. In L1L, Sr (10–21 ppm, avg. 12 ± 4 ppm) and Rb (26–34 ppm, avg. 27 ± 4 ppm) differ slightly from the younger lavas that taken together (*n* = 617) have compositions of Sr (1–81 ppm, avg. 7 ± 10 ppm), and Rb (22–94 ppm, avg. 52 ± 30 ppm). The most significant difference between L1L and the other lavas is found in Ba with L1L having an order of magnitude more Ba (429–750 ppm, avg. 685 ± 120 ppm) in sanidine than the other lavas (4–54 ppm, avg. 23 ± 28 ppm).

#### 4.4. Oxygen isotopes

Feldspar δ<sup>18</sup>O values for the lavas measured in this study range from 6.77 to 5.42 ‰ (data in supplementary material). Where multiple samples of the same lava were analysed, reproducibility ranges from excellent (in the case of U8L, std. dev. = 0.03 ‰) to acceptable (in the case of U11L, std. dev. = 0.23 ‰). The feldspar lava data overlap with the ranges of values from the surrounding ignimbrites (Fig. 8; Cortes-Calderon et al., 2022). Interestingly, the L1L unit, the lowest of the units considered to represent the Fataga succession by Cortes-Calderon et al. (2022) has the highest δ<sup>18</sup>O value, which is similar to the underlying Mogán units (Fig. 8).

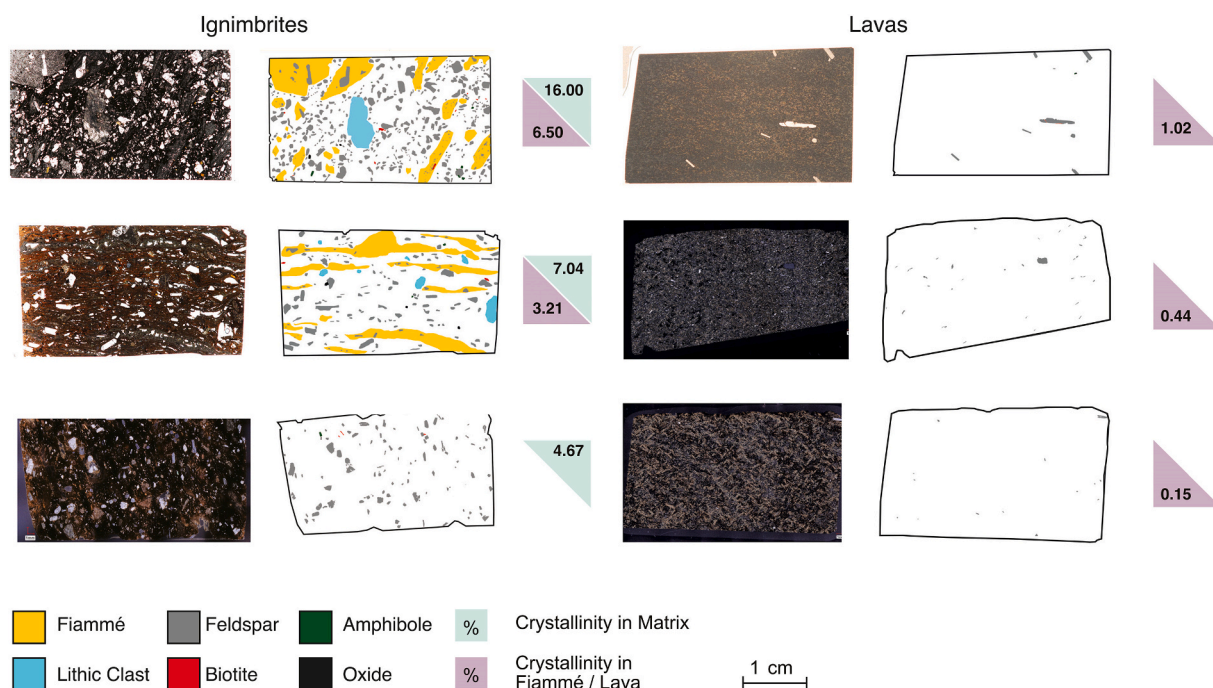
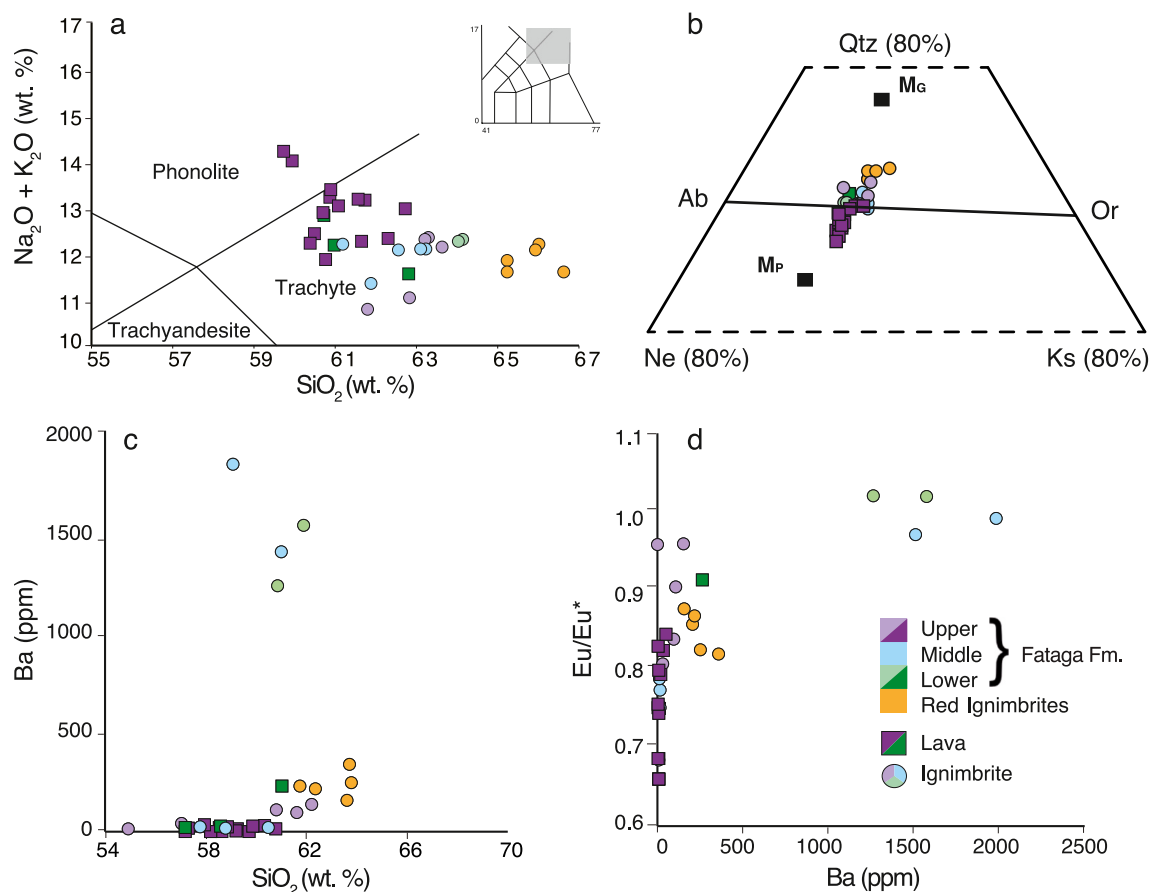


Fig. 3. Thin section images with measured crystallinity from lavas and ignimbrites illustrating the nearly aphyric nature of the lavas.



**Fig. 4.** Bulk rock compositions of Fataga lavas from this study and ignimbrites from Cortes-Calderon et al. (2022). A. TAS plot showing the classification (after Le Bas et al., 1986) of lavas and ignimbrites. B. Illustration of the positions of the lavas and individual juvenile clasts in normative quartz-nepheline-kalsilite 'petrogeny's residua system' at 1 bar with the shift to silica-undersaturated compositions in the upper Fataga.  $M_G$  and  $M_P$  indicate the granite and phonolite minimum respectively (following Tuttle and Bowen, 1958; Hamilton and MacKenzie, 1965). C. and D. Trace elemental (Ba, Eu) indicators of the involvement of feldspar-dominated cumulates occurring within the ignimbrites.

#### 4.5. Lead isotopes

Pb isotopic compositions of the large feldspars from Fataga lavas span the range of 39.54–39.69 in  $^{208}\text{Pb}/^{204}\text{Pb}$ , 15.60–15.62 in  $^{207}\text{Pb}/^{204}\text{Pb}$ , and 19.77–19.96 in  $^{206}\text{Pb}/^{204}\text{Pb}$  (all new data in supplementary materials). The lava values are similar to both our new data from Fataga ignimbrites and to the published Fataga data (Cousens et al., 1990). Overall, these compositions record a shift through time to higher  $^{206}\text{Pb}/^{204}\text{Pb}$  (Fig. 9). Interestingly, the shift in Pb isotopic compositions observed between Mogán and Fataga appears to occur between the L3P and L5L units, suggesting that these units constitute the most appropriate division between Mogán and Fataga magmas. Based on the ages of Cortes-Calderon et al. (2022) this is occurring sometime between 12.427 and 11.857, while in the Van den Bogaard and Schmincke (1998) stratigraphy, the first 'Fataga' unit that they refer to is 12.4 Ma (recalculated to the same monitor age). This change in Pb isotope composition is also coincident with a change in O isotopic composition.

## 5. Discussion

### 5.1. How related are Fataga ignimbrites and lavas?

Throughout the Fataga stratigraphy, erupted crystal-poor material ranges from trachytic to phonolitic, with lava samples being slightly more alkaline in composition, up to phonolitic in some of the upper lavas (Fig. 4). In addition to the crystal-poor material, a number of the ignimbrites also exhibit co-erupted crystal-rich juvenile clasts that are

predominantly found in the late-erupted portions of the deposits. These crystal-rich juveniles are trachytic in bulk composition and have glass compositions that show elevated Ba and have  $\text{Eu}/\text{Eu}^*$  values above 1 (Cortes-Calderon et al., 2022). Similar bulk compositions are not found in any of the lavas studied here. The generation of these geochemical signatures has been widely invoked as resulting from the interaction of recharge magmas with a feldspar-dominated cumulate (e.g., Wolff et al., 2020; Forni et al., 2016; Foley et al., 2020; Deering et al., 2011). This process is particularly obvious in alkaline systems whereby the near-monomineralic nature of syenitic cumulates effectively pulls the composition towards trachyte (Wolff, 2017). On a crystal scale, while the major elemental composition of the feldspars is similar in lava samples, crystal-poor juveniles and crystal-rich juveniles in ignimbrites (Fig. 7) have markedly different trace element compositions. In the lavas, Ba contents of feldspars never reach higher than 900 ppm (L1L), while in the ignimbrites, feldspar Ba contents may be orders of magnitude higher (Fig. 7). The lavas, therefore, preserve no evidence for cumulate remelting while such remelting is obvious in some pumices present in ignimbrites (particularly in late-erupted material).

Isotopically, the coherent variations in Pb and O isotopic ratios (Fig. 10) throughout the Fataga volcanism indicate that the magmas feeding both the ignimbrites and lavas have a common source despite their petrographic differences. The trend of higher  $^{206}\text{Pb}/^{204}\text{Pb}$  and  $^{208}\text{Pb}/^{204}\text{Pb}$  ratios with increasing stratigraphic height (Fig. 9) is consistent with an increasing importance for a HIMU-like (elevated U and Th values compared to Pb; Zindler and Hart, 1986) source over the course of Fataga magmatism. Whether this is due to the influx of a new

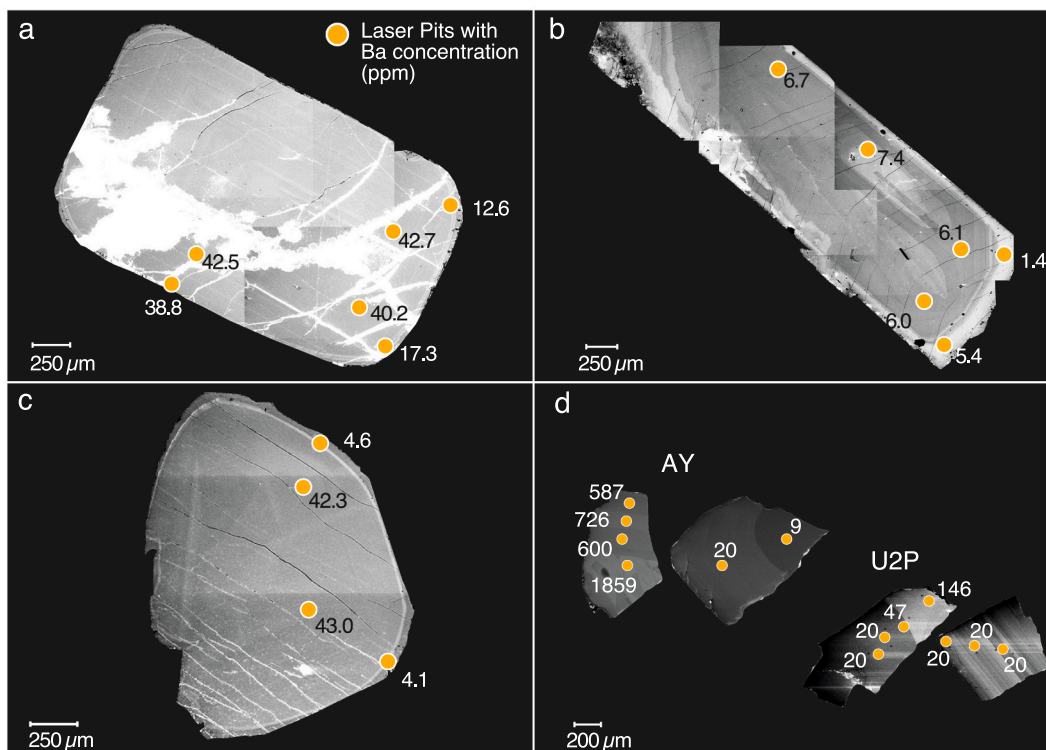


Fig. 5. Cathode luminescence (CL) images showing limited zonation within the large sanidine crystals compared to those from the ignimbrites. Ba contents (ppm) illustrated with numbers. A., B. & C: U5L lavas, D: Ignimbrites AY and U2P from Cortes-Calderon et al. (2022).

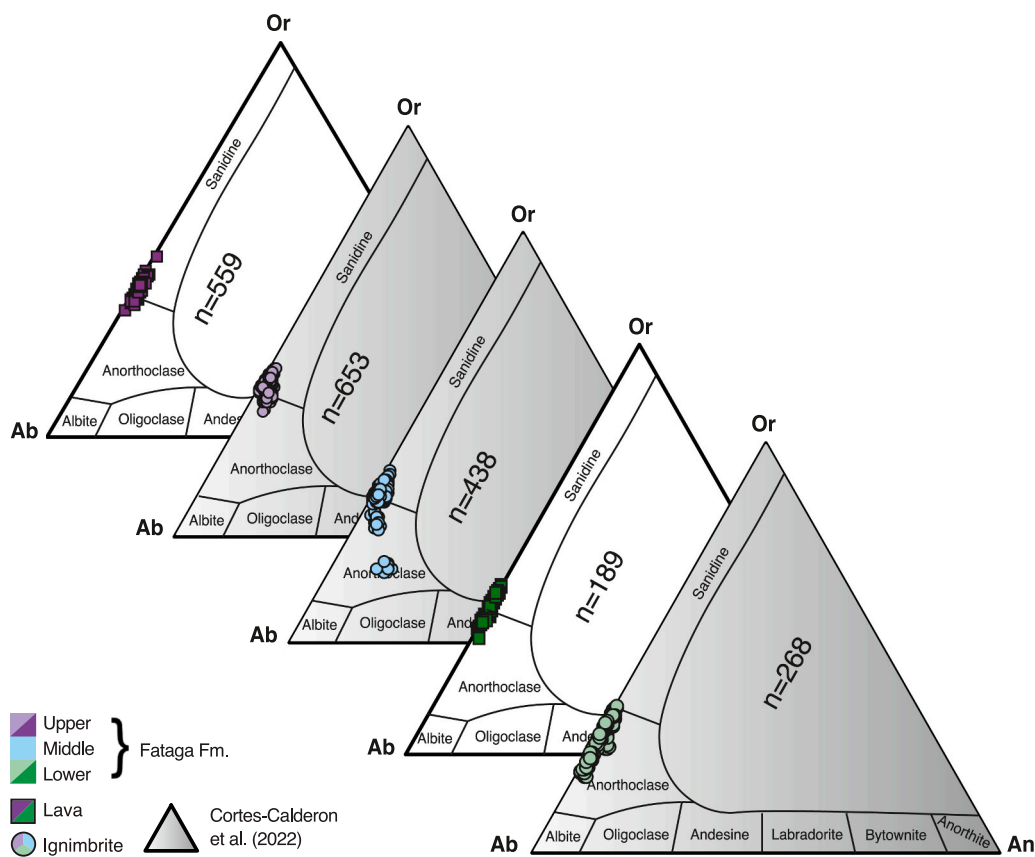


Fig. 6. Major elemental compositions of feldspars from the Fataga units in the  $KAlSi_3O_8$  (Or)-anorthite (an)-albite (ab) ternary diagram compared to the ignimbrite compositions from the same stratigraphic horizon (ignimbrite data from Cortes-Calderon et al., 2022).



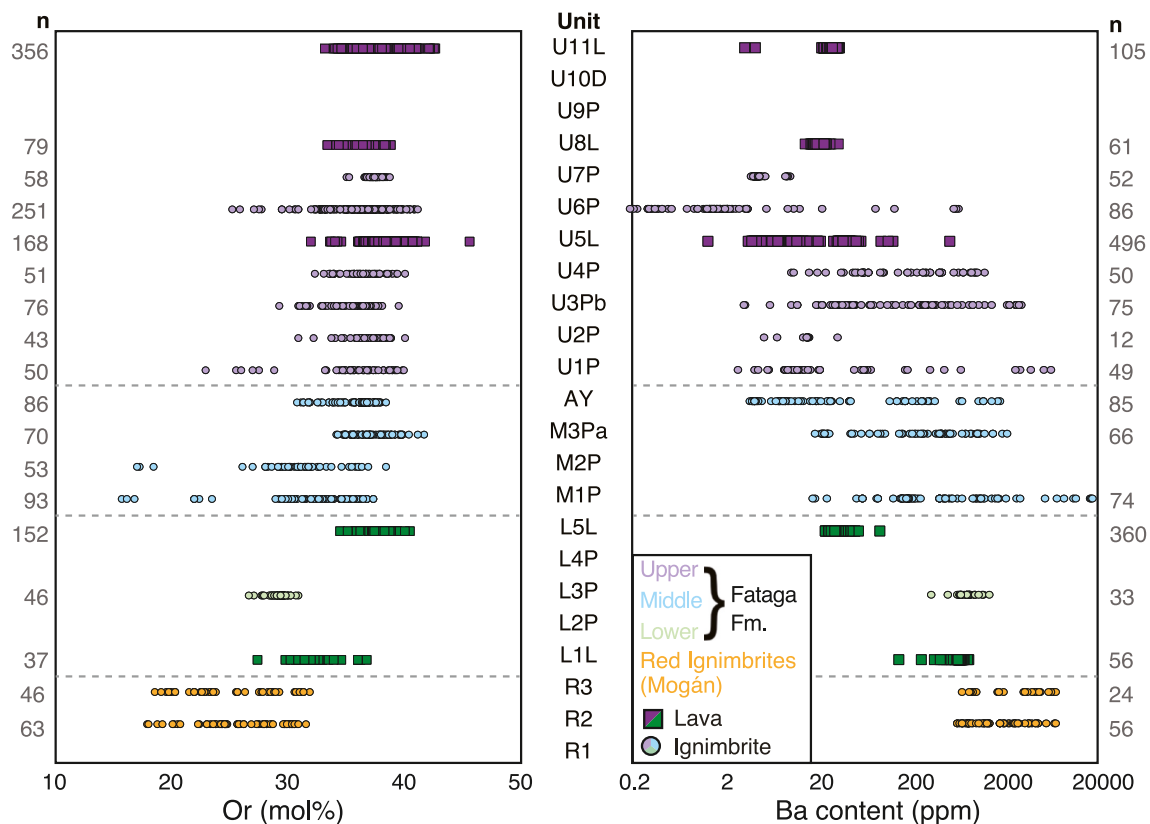
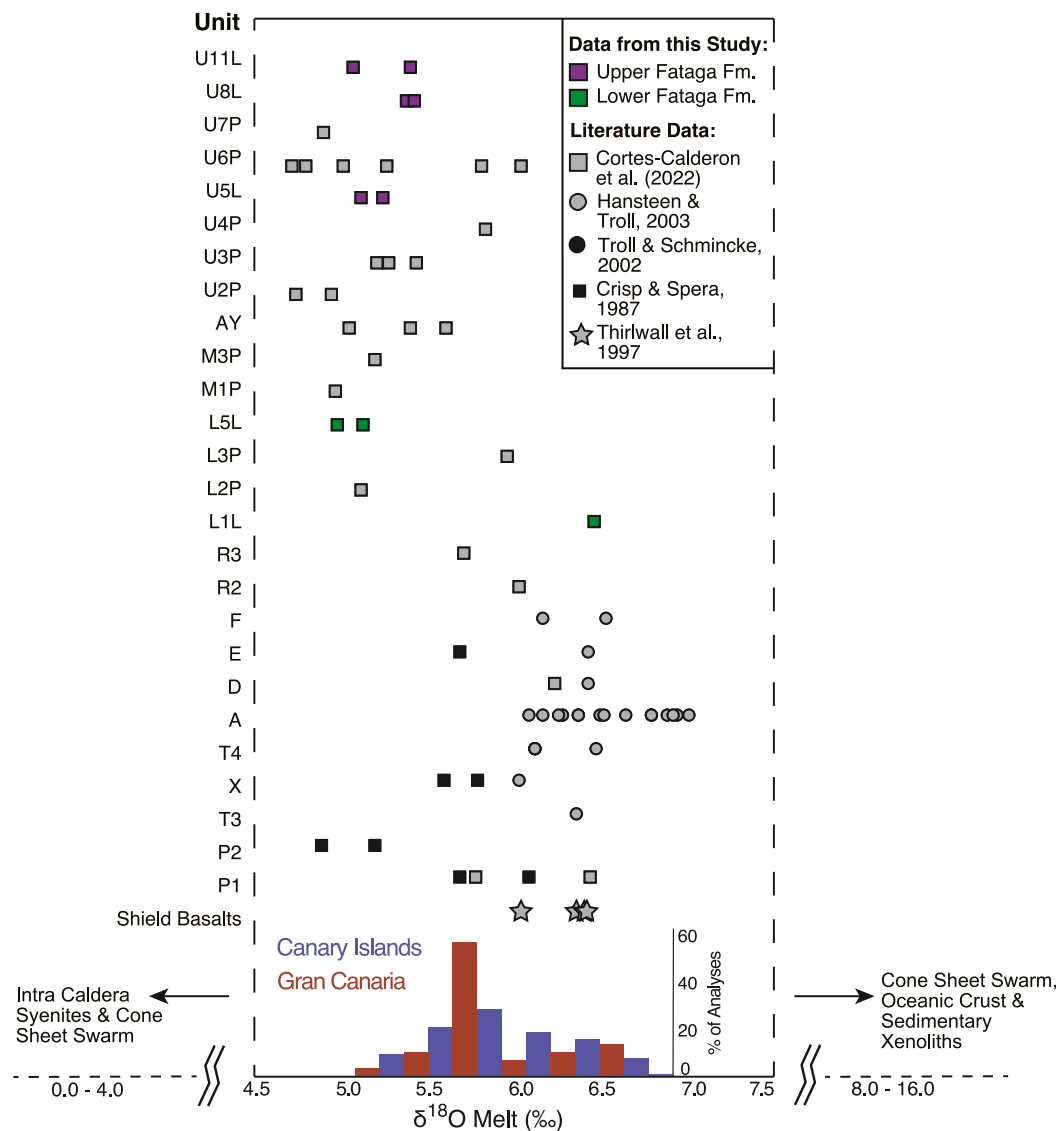


Fig. 7. Feldspar compositions throughout the Fataga stratigraphy showing the change in compositions through time. The variability within ignimbrite samples (e.g., U6P) may be much greater than that observed in the lavas. Note that the axis for the Ba plot is logarithmic. Lava data are from this study and ignimbrite data from Cortes-Calderon et al. (2022).

magma ‘blob’ into the magmatic system (e.g., Hoernle and Schmincke, 1993) or exhaustion of other ingredients in the sub-Canarian magmatic cocktail acting to promote this high  $^{206}\text{Pb}/^{204}\text{Pb}$  component remains unclear. Cousens et al. (1990) inferred the up-succession compositional change as the arrival of a new ‘Fataga magma’. The lack of primitive magmas erupted within the Fataga sequence acts to complicate understanding of potential mantle sources. However, a trend in the direction of increasing  $^{206}\text{Pb}/^{204}\text{Pb}$  is hard to ascribe to a source within the crust as most of the preceding Shield and Mogán volcanism erupted compositions with lower  $^{206}\text{Pb}/^{204}\text{Pb}$  ratios.

The decreasing  $\delta^{18}\text{O}$  values with stratigraphic height provide another constraint on petrogenesis. Closed-system fractionation from mafic parental magmas is thought to impart an increase of  $\delta^{18}\text{O}$  on the order of 0.5 per mil or more, depending on the mineral assemblage involved in the liquid line of descent (as illustrated by Bucholz et al., 2017). The magmatic values reaching as low as 4.76 ‰ (Cortes-Calderon et al., 2022) in the evolved Fataga suite would therefore require a parental, mafic magma with a  $\delta^{18}\text{O}$  value of around 4.20 ‰ or less (Fig. 8). Published and recalculated melt O isotopic compositions of mafic samples, however, only go as low as 5.16 ‰ (average: 5.66 ‰) for Gran Canaria and 5.02 ‰ (average: 5.73 ‰) for the whole Canarian archipelago (Fig. 8). The absence of such primitive magmas implies that the subtly low  $\delta^{18}\text{O}$  values of the Fataga volcanics are inherited as the magmas traverse the crust. In an ocean island setting, the diversity of potential assimilants is relatively limited. Of those characterised, the quartz-rich sediments of layer 1 of the ocean crust have bulk  $\delta^{18}\text{O}$  values above 14 ‰ (Hansteen and Troll, 2003) and the hydrothermally altered volcanic rocks within the Tejada caldera have bulk  $\delta^{18}\text{O}$  11.9–18.4 ‰ (Donoghue et al., 2008) conclusively excluding these as sources to lower the  $\delta^{18}\text{O}$  value in the Fataga magmas. The altered igneous components of the oceanic crust beneath the Canaries range from 3.3 to 8.6 ‰ with

an overall average  $\delta^{18}\text{O}$  of 5.1 ‰ (Hansteen and Troll, 2003) so would have limited leverage as assimilant. A more likely alternative would be hydrothermally altered intrusive rocks at shallow levels within the volcanic plumbing system, with the cone sheets having an average  $\delta^{18}\text{O}$  of 4.7 ‰ ( $n = 23$ ) and three samples of syenites having an average  $\delta^{18}\text{O}$  of 1.6 ‰ (Donoghue et al., 2010). Indeed, such hydrothermally altered intrusive rocks have been reported from across the archipelago (Javoy et al., 1986; Wolff et al., 2000; Donoghue et al., 2010) with suitable O isotopic characteristics (average  $\delta^{18}\text{O} = 3.13$  ‰, median  $\delta^{18}\text{O} = 2.50$  ‰,  $n = 83$ ). Taking the lowest  $\delta^{18}\text{O}$  bulk rock from the Javoy et al. (1986) compilation (a microsyenite from Fuerteventura at  $-0.4$  ‰) implies around 10% assimilation, while taking the average of the syenites from Donoghue et al. (2010) implies 15–20% assimilation. Such values are consistent with other studies (Farmer et al., 1991; Bindeman et al., 2004; Troch et al., 2018) particularly for ocean island settings (e.g., Geist et al., 1998; Ellis et al., 2022). Within the Fataga samples there is a weak correlation between O and Pb isotopic compositions (Fig. 10). However, it is notable that the Fataga samples are distinct from the underlying Mogán compositions (Figs. 8, 9). The consistently high  $^{206}\text{Pb}/^{204}\text{Pb}$  (previously interpreted as a changing composition in mantle input, Cousens et al., 1990; Hoernle and Schmincke, 1993) implies a limited role for Mogán materials in Fataga genesis. Rather, it suggests that the hydrothermally altered materials (as required by the O isotopes) are Fatagan in Pb isotopic character. These hydrothermally altered, relatively young crystalline or ‘mushy’ materials would be at higher temperature relative to the older, cooled Mogán intrusives and thus more prone to melting (e.g., Bacon et al., 1989). The absence of primitive magmas within the Fataga suite (as potential parental compositions) and the lack of Pb isotopic data for potential assimilants characterised for  $\delta^{18}\text{O}$  precludes development of a more sophisticated mixing model.



**Fig. 8.** Oxygen isotope composition of the volcanic products ( $\Delta_{\text{feldspar} - \text{magma}} = +0.3\%$  after Harris et al., 1999) on Gran Canaria. The lava data from the Fataga succession are in good agreement with the existing data from the surrounding ignimbrites (Cortes-Calderon et al., 2022) and show a decrease in  $\delta^{18}\text{O}$  with increasing stratigraphic height following the earlier Mogán volcanism. Uncertainties on our O isotopic measurements are  $\pm 0.16\%$  with literature uncertainties similar. Arrows on diagram show potential assimilant values and bar chart at base shows compiled recalculated melt  $\delta^{18}\text{O}$  values of shield basalts in Gran Canaria ( $n = 25$ ) and the Canary Islands in general ( $n = 161$ ) illustrating no mafic magmas (with the exception of a single peridotite value of 4.36‰ reported by Day et al., 2010) are known that could be directly parental to the Fataga compositions. Literature data from Thirlwall et al. (1997), Crisp and Spera (1987), Troll and Schmincke (2002), Hansteen and Troll (2003), Gurenko et al. (2006, 2011), Day et al. (2010), Cortes-Calderon et al. (2022).

## 5.2. Origin of the big crystals in lavas

The unusually large feldspar crystals within an otherwise crystal-poor lava raises the question of whether they are likely to be phenocrystic or inherited from other sources. Intrusive rocks are exposed in the interior of Gran Canaria with a cone sheet swarm documented by Schmincke (1967). However, these cone sheets were emplaced after the main phase of Fataga volcanism (Schirnack et al., 1999) and so cannot be an origin for the megacrysts. Syenitic fragments occur as lithic clasts throughout both the Mogán and Fataga ignimbrite successions (Sumner and Branney, 2002; Schmincke and Sumita, 1998; Cortes-Calderon et al., 2022) even in the first explosive deposit, P1 (Freundt and Schmincke, 1998). The presence of syenitic lithic clasts even in P1 establishes that evolved compositions were already present in the magmatic plumbing system right at the onset of trachytic / phonolitic volcanism. Only the syenitic clasts in P1 have been studied in detail on

Gran Canaria (Freundt-Malecha, 2001) and these are referred to as ‘quartz trachytes’ from the earlier, silica-saturated, Mogán era of volcanism. The neighbouring island of Tenerife however, has nepheline-syenite clasts that are related to phonolitic activity and may provide a better framework for comparison (Wolff, 1987). Such nepheline syenites appear unlikely to be a source for the megacrysts for a number of reasons: i) by proportion feldspar is ca. 65% by volume with a range of other phases co-occurring. These other phases are not found within the Fataga lavas, ii) most of the syenitic feldspars show microcline exsolution textures that are absent in our samples (as illustrated in elemental maps, supplementary fig. 1), iii) many of the feldspars in the syenites are visibly altered, and iv) all of the syenitic feldspar crystals show an albitic rim that we have not observed in the Fataga crystals. Rather, we consider the euhedral megacrysts to be phenocrysts within the lavas.

Feldspar crystals significantly larger than other co-occurring phases (megacrysts) have been widely reported from intrusive suites in a range

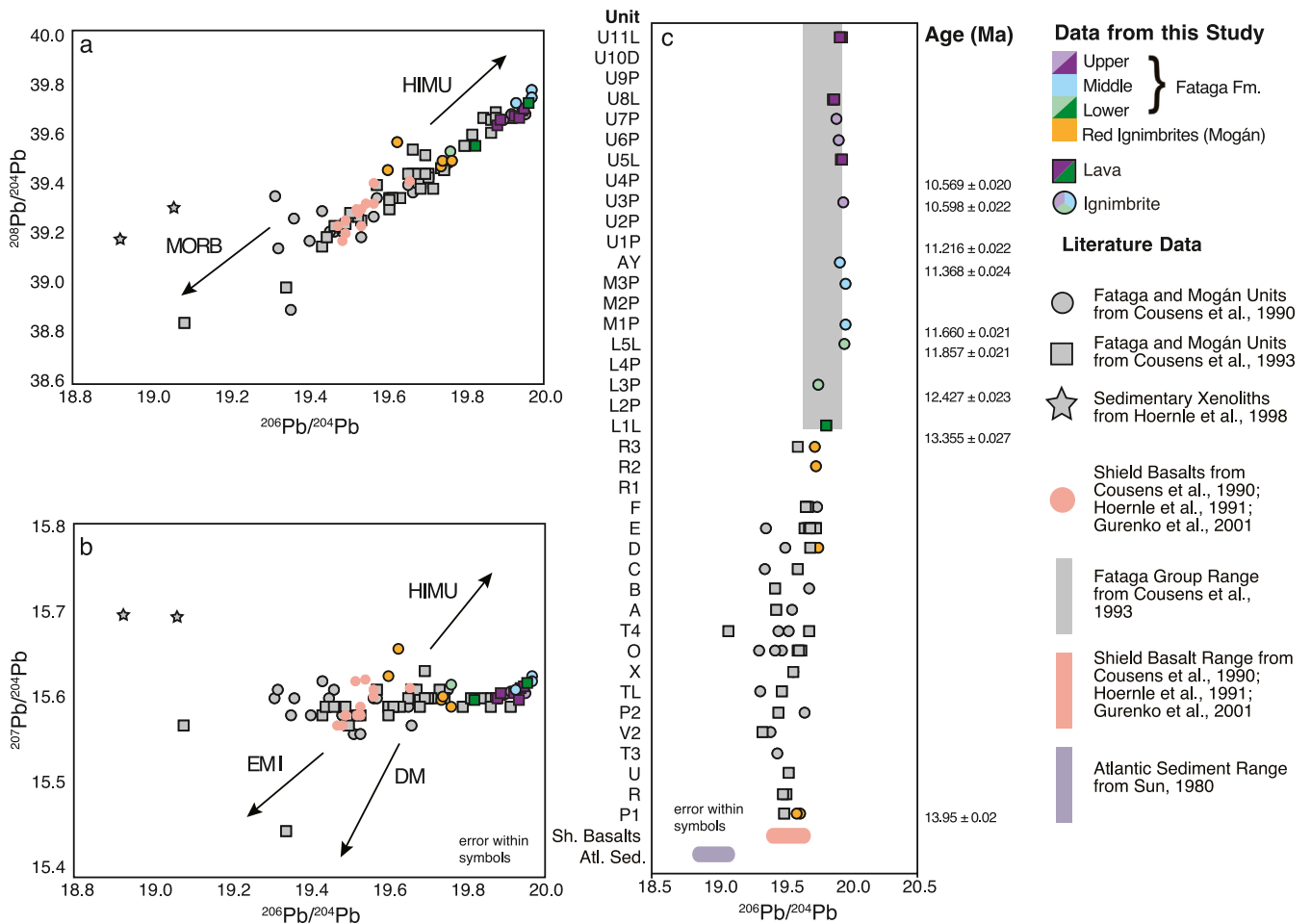


**Fig. 9.** Pb isotopic composition of the Fataga deposits. A. and B.  $^{208}\text{Pb}/^{204}\text{Pb}$  (error:  $\pm 0.08$ ) and  $^{207}\text{Pb}/^{204}\text{Pb}$  plots vs.  $^{206}\text{Pb}/^{204}\text{Pb}$  showing the similarity of compositions between the lavas and ignimbrites within the Fataga and a limited role for sedimentary material during petrogenesis. C. Increasing  $^{206}\text{Pb}/^{204}\text{Pb}$  through the Miocene record of Gran Canaria confirming the trend reported by Cousens et al. (1990). Agreement between our results and published data is illustrated in the P1 and D ignimbrites. Other literature data are from Sun (1980), Hoernle et al. (1991), Cousens et al. (1993), Hoernle (1998) and Gurenko et al. (2001). Ages of Fataga units are from Cortes-Calderon et al. (2022) and P1 from Van den Bogaard and Schmincke (1998).

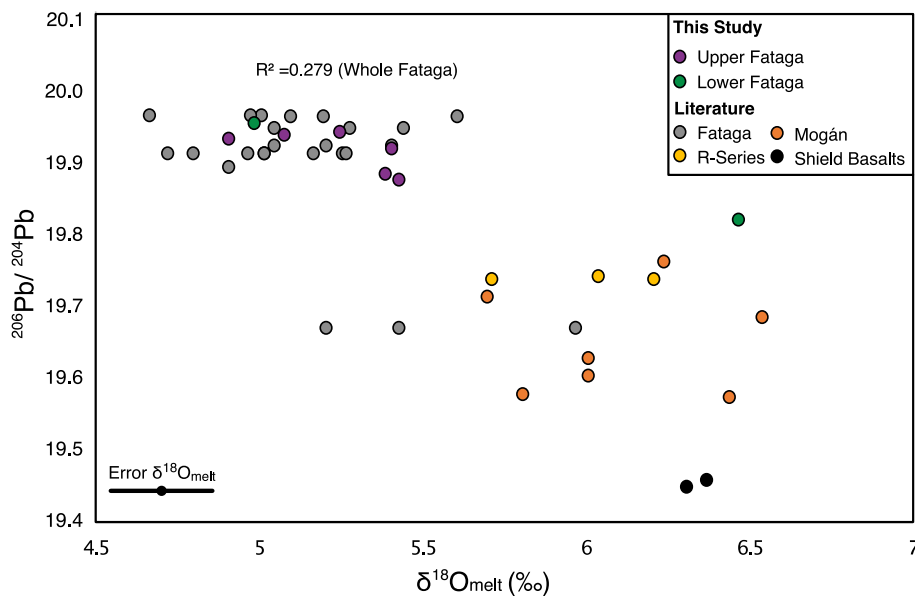


**Fig. 10.** Lead vs. oxygen isotope compositions of Miocene felsic volcanic rocks and shield basalts from Gran Canaria. Pb errors are within symbol size.

of settings (e.g., Elba, Farina et al., 2010; Tuolumne, Johnson and Glazner, 2010; amongst many) where they have been often interpreted as reflecting Ostwald ripening processes via temperature cycling (Johnson and Glazner, 2010). In volcanic rocks, such megacrysts appear less frequent with prominent examples seemingly limited to a relatively small number of locations (e.g., Fish Canyon Tuff, Bachmann et al., 2002; Taapaca, Higgins, 2011, Rout et al., 2021; Erebus, Moussallam et al., 2015; Mt. Amiata, Landi et al., 2019). In volcanic systems, these outsized feldspars typically exhibit a complex record of resorption, regrowth, and entrapment of other mineral phases and/or melt (Fig. 11) with this textural complexity accompanied by intracrystal compositional variability. The large Fataga lavas contain few if any melt inclusions, limited textural variability in CL images (Fig. 5) and limited compositional zonation in major or trace elements (Figs. 6, 7) when compared to the feldspars from the ignimbrites (Fig. 7).

As is widely known by experimental petrologists, thermal cycling by relatively small amounts around a fixed point is an effective method for enlarging crystals. Indeed, this small temperature cycling (on the order of  $\pm 10$  °C) in both synthetic (Mills et al., 2011) and natural systems (Mills and Glazner, 2013) increases crystal sizes by up to orders of magnitude in short duration experiments (140 h or less). Given that timescales of pre-eruptive magmatic residence are typically quoted in units of thousands of years (Szymanowski et al., 2017; Rout and Wörner, 2020) such processes may play an important role. For the megacrystic sanidines of Taapaca that exhibit limited major elemental variability, Rout et al. (2021) invoked a ‘thermal mixing’ model (after Couch et al., 2001 and Ruprecht and Wörner, 2007), whereby either small proportions of recharge or distal recharge produced only limited chemical effects on the megacryst-hosting magma. The transfer of heat and volatiles between magmas (without significant mass transfer) may occur in both silicic (e.g., Wolff et al., 2015) and mafic (e.g., Spilliaert et al., 2006) settings. The major element homogeneity and only limited trace

element variation within the Fataga lavas would be consistent with a similar scenario occurring on Gran Canaria with recharge (the effects of which are observable in the crystal-rich juveniles e.g., Fig. 4) transferring mostly heat and volatiles and primarily affecting the core of the magmatic system. Significant thermal cycling promotes trapping of melt inclusions in crystals by strong changes in crystal growth rate or by crystal dissolution/re-crystallisation (Audétat and Lowenstern, 2014). A more peripheral storage zone would favour a smaller amplitude in the thermal cycling, and a more constant growth of feldspar crystals, hindering melt inclusions entrapment as observed in megacrysts from Fataga lavas.

### 5.3. Flank eruptions vs central vent eruptions

The lavas in this study are petrographically distinct from their explosively erupted counterparts and, from their appearance within our field area (and supported by the distribution of lavas in larger scale geological maps of the island, Balcells-Herrera et al., 1992) were seemingly erupted from sources outside the Tejeda caldera. The lateral transport of magma in the shallow crust has been observed in many volcanic systems (e.g., Etna, Metrich et al., 2004; San Juan Volcanic Field, Sliwinski et al., 2019; Kilauea, Wieser et al., 2022) and in many cases the magma found in these rift zones may differ geochemically or petrographically from that within the main volcanic edifice (e.g., dacitic magmas stored in the rift zones of Kilauea, Wieser et al., 2022). Here we propose that the magmas that formed the Fataga lavas were stored sufficiently distal from the main reservoir to escape the fluctuations resulting from recharge and cumulate melting but close enough to maintain high enough temperatures to remain above the solidus (Fig. 12). The increasing realisation of the potential for such ‘rogue’ magma batches to exist, and in the case of Fataga magmatism repeatedly erupt, provides new impetus to investigate the potential hazards

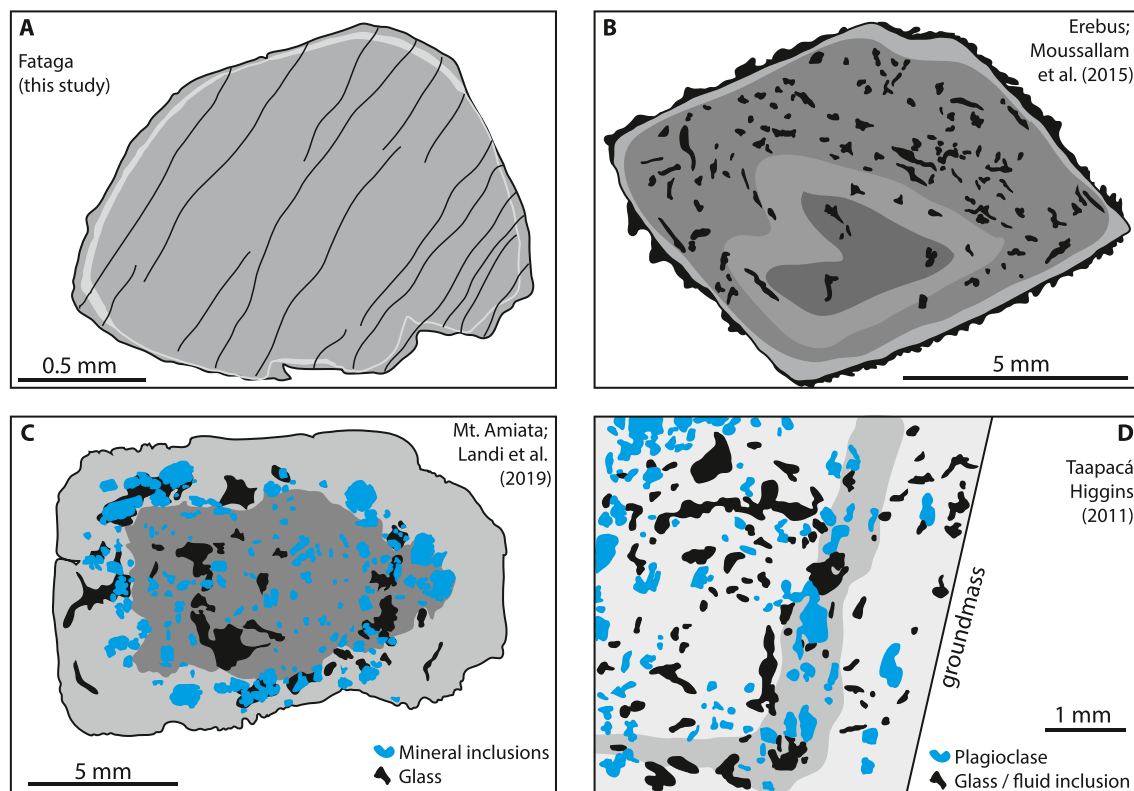
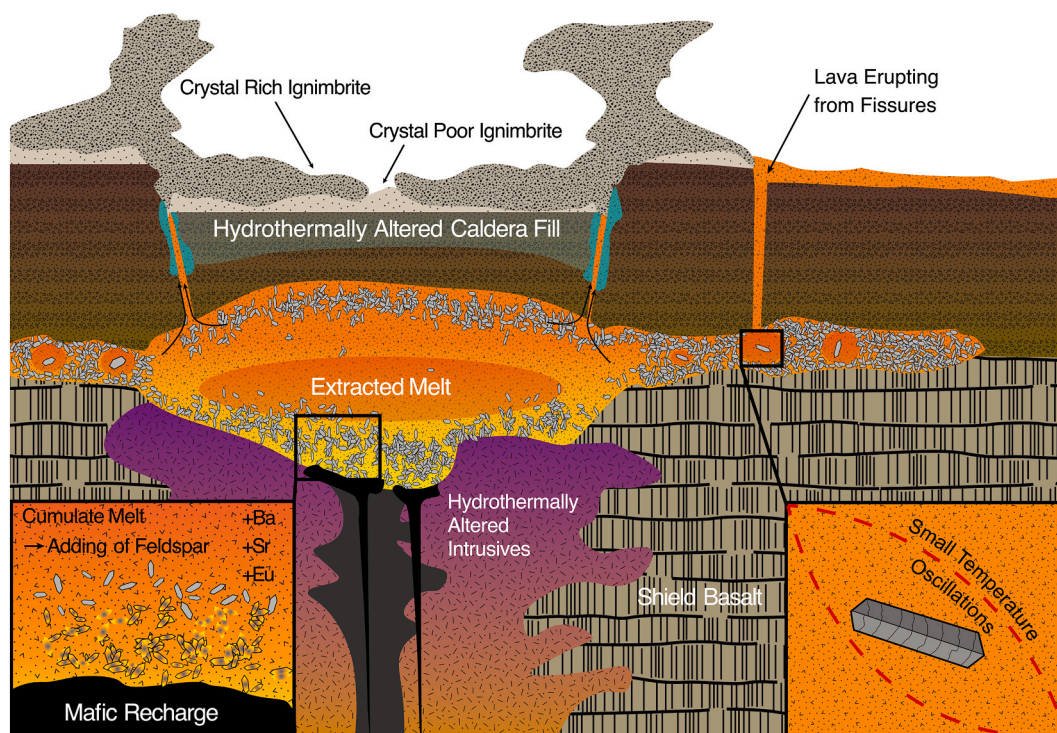


Fig. 11. Appearance of large sanidine crystals in Gran Canaria lavas compared to other volcanic units. A. Lava L5L (Fig. 5), B. Erebus, Moussallam et al. (2015), C. Mt. Amiata, Landi et al. (2019), and D. Taapaca, Higgins (2011). The internal zonation of the sanidines is for illustration as the original diagrams used a variety of image types (e.g., compositional maps of K, CL imaging).



**Fig. 12.** Sketch illustrating the proposed magmatic environment of both the Fataga ignimbrites and lavas. The main intra caldera reservoir allows for fractional crystallisation and episodic mafic recharge and thus cumulate involvement and adding of feldspar. The peripheral extra caldera reservoir experiences only slight temperature oscillations in consequence and allows for sanidine megacryst growth.

resulting from eruption on the typically more populated lower slopes of active volcanoes.

## 6. Conclusions

The main conclusions of our study are:

- i) During Miocene volcanism on Gran Canaria, explosive eruptions from the Tejeda caldera alternated with effusions of compositionally similar lavas from extra-caldera sources.
- ii) The lavas have compositions that approximate those of the crystal-poor juveniles of the ignimbrites, both representing extracted melts from a larger magmatic reservoir. Despite their geochemical similarities, the lavas are petrographically distinct, containing large (cm-scale) sanidine crystals but few if any other phases. This reflects a case where the explosive-effusive transition is clearly expressed in the petrographic record.
- iii) The crystal-rich juveniles from the ignimbrites are interpreted to reflect processes of cumulate melting and entrainment during larger explosive eruptions. These signatures are absent in the lavas.
- iv) O isotopic compositions reveal that the lavas and ignimbrites within the Fataga group are following the same overall trend, to lower  $\delta^{18}\text{O}$  values with increasing stratigraphic height. This lowering of  $\delta^{18}\text{O}$  is inferred to reflect a contribution from assimilation of hydrothermally altered syenites at depth within the edifice.
- v) Pb isotopes from the lavas and ignimbrites show an increase in  $^{206}\text{Pb}/^{204}\text{Pb}$  stratigraphically upwards, reflecting a change in dominant mantle sources towards a HIMU dominated component over time in agreement with previous studies.
- vi) The isotopic similarity yet petrographic differences between Fataga ignimbrites and lavas leads us to propose a model whereby the magmas share a deeper source that controls their isotopic

character but were stored in slightly different conditions in the shallow crust. The extra-caldera sources of the lavas reflect storage of these magmas separately from the main crustal reservoir with buffered temperatures promoting the growth of large sanidine crystals that exhibit limited evidence for interaction with more mafic recharge magma.

## Declaration of Competing Interest

The authors declare the following financial interests/personal relationships which may be considered as potential competing interests:

Ben Ellis reports financial support was provided by Swiss National Science Foundation.

## Data availability

Electronic Appendix provided with the manuscript

## Acknowledgements

We gratefully acknowledge partial funding support from the Swiss National Science Foundation (200020\_197040 to BE) and Grubenmann-Burri funds from ETH Zurich. DS was supported by U.S. NSF award EAR-1735512. Lydia Zehnder and Marcel Guillong provided typically superb support for analytical work. Constructive journal reviews were kindly provided by Karoly Nemeth and Nicole Métrich, and editorial assistance was provided by Claudia Romano.

## Appendix A. Supplementary data

Supplementary data to this article can be found online at <https://doi.org/10.1016/j.chemgeo.2022.121242>.

## References

- Abdel-Monem, A., Watkins, N.D., Gast, P.W., 1971. Potassium-argon ages, volcanic stratigraphy, and geomagnetic polarity history of the Canary Islands; Lanzarote, Fuerteventura, Gran Canaria, and La Gomera. *Am. J. Sci.* 271 (5), 490–521.
- Abdel-Monem, A., Watkins, N., Gast, P.W., 1972. Potassium-argon ages, volcanic stratigraphy, and geomagnetic polarity history of the Canary Islands; Tenerife, La Palma and Hierro. *Am. J. Sci.* 272 (9), 805–825.
- Adams, N.K., Houghton, B.F., Fagents, S.A., Hildreth, W., 2006. The transition from explosive to effusive eruptive regime: the example of the 1912 Novarupta eruption, Alaska. *Geol. Soc. Am. Bull.* 118 (5–6), 620–634.
- Audétat, A., Lowenstern, J.B., 2014. Melt Inclusions. *Geochemistry of Mineral Deposits*. Elsevier, Amsterdam, pp. 143–173.
- Bachmann, O., Dungan, M.A., Lipman, P.W., 2002. The fish Canyon Magma Body, San Juan Volcanic Field, Colorado: Rejuvenation and Eruption of an Upper-Crustal Batholith. *J. Petrol.* 43 (8), 1469–1503.
- Bacon, C.R., Adams, L.H., Lanphere, M.A., 1989. Direct evidence for the origin of low- $^{18}\text{O}$  silicic magmas: quenched samples of a magma chamber's partially-fused granitoid walls, Crater Lake, Oregon. *Earth Planet. Sci. Lett.* 96 (1–2), 199–208.
- Balcells-Herrera, R., Barrera-Morale, J.L., Gómez-Sainz de Aja, J.A., 1992. Mapa Geológico de España a escala 1:100.000: Isla de Gran Canaria. Instituto Tecnológico GeoMinero de España, Madrid.
- Bindeman, I.N., Ponomareva, V.V., Bailey, J.C., Valley, J.W., 2004. Volcanic arc of Kamchatka: a province with high- $\delta^{18}\text{O}$  magma sources and large-scale  $^{18}\text{O}/^{16}\text{O}$  depletion of the upper crust. *Geochim. Cosmochim. Acta* 68, 841–865.
- Bucholz, C.E., Jagoutz, O., VanTongeren, J.A., Setera, J., Wang, Z., 2017. Oxygen isotope trajectories of crystallizing melts: Insights from modeling and the plutonic record. *Geochim. Cosmochim. Acta* 207, 154–184.
- Carracedo, J.C., Troll, V.R., 2016. *The Geology of the Canary Islands*. Elsevier, Amsterdam, Netherlands. <https://doi.org/10.1016/C2015-0-04268-X>.
- Cassidy, M., Manga, M., Cashman, K., Bachmann, O., 2018. Controls on explosive-effusive volcanic eruption styles. *Nat. Commun.* 9 (1), 1–16.
- Christiansen, R.L., 2001. The Quaternary and Pliocene Yellowstone Plateau Volcanic Field of Wyoming, Idaho, and Montana (Vol. 729). US Department of the Interior, US Geological Survey.
- Cortes-Calderon, E.A., Ellis, B.S., Harris, C., Mark, D., Neukampf, J., Wolff, J.A., Ulmer, P., Bachmann, O., 2022. Generation and field relations of low- $\delta^{18}\text{O}$  silica-undersaturated and mildly saturated alkaline magmas: A case study from the Fataga Group, Gran Canaria. *J. Petrol.* 63 (9), 1–22. <https://doi.org/10.1093/ptrology/egac090>.
- Couch, S., Sparks, R.S.J., Carroll, M.R., 2001. Mineral disequilibrium in lavas explained by convective self-mixing in open magma chambers. *Nature* 411, 1037–1039.
- Cousens, B.L., Spera, F.J., Tilton, G.R., 1990. Isotopic patterns in silicic ignimbrites and lava flows of the Mogán and lower Fataga formations, Gran Canaria, Canary Islands: Temporal changes in mantle source composition. *Earth Planet. Sci. Lett.* 96 (3–4), 319–335.
- Cousens, B.L., Spera, F.J., Dobson, P.F., 1993. Post-eruptive alteration of silicic ignimbrites and lavas, Gran Canaria, Canary Islands: Strontium, neodymium, lead, and oxygen isotopic evidence. *Geochim. Cosmochim. Acta* 57 (3), 631–640.
- Crisp, J.A., Spera, F.J., 1987. Pyroclastic flows and lavas of the Mogán and Fataga formations, Tejada Volcano, Gran Canaria, Canary Islands: mineral chemistry, intensive parameters, and magma chamber evolution. *Contrib. Mineral. Petrol.* 96 (4), 503–518.
- Day, J.M., Pearson, D.G., Macpherson, C.G., Lowry, D., Carracedo, J.C., 2010. Evidence for distinct proportions of subducted oceanic crust and lithosphere in himu-type mantle beneath El Hierro and La Palma, Canary Islands. *Geochim. Cosmochim. Acta* 74 (22), 6565–6589.
- Deering, C.D., Bachmann, O., Dufek, J., Gravelly, D.M., 2011. Rift-related transition from andesite to rhyolite volcanism in the Taupo Volcanic Zone (New Zealand) controlled by crystal-melt dynamics in mush zones with variable mineral assemblages. *J. Petrol.* 52 (11), 2243–2263.
- Di Genova, D., Kolzenburg, S., Wiesmaier, S., Dallanave, E., Neuville, D.R., Hess, K.U., Dingwell, D.B., 2017. A compositional tipping point governing the mobilization and eruption style of rhyolitic magma. *Nature* 552, 235–238.
- Donoghue, E., Troll, V.R., Harris, C., O'Halloran, A., Walter, T.R., Torrado, F.J.P., 2008. Low-temperature hydrothermal alteration of intra-caldera tuffs, Miocene Tejada caldera, Gran Canaria, Canary Islands. *J. Volcanol. Geotherm. Res.* 176 (4), 551–564.
- Donoghue, E., Troll, V.R., Harris, C., 2010. Fluid–rock interaction in the miocene postcaldera, Tejada intrusive complex, Gran Canaria (Canary Islands): Insights from mineralogy, and o-and h-isotope geochemistry. *J. Petrol.* 51 (10), 2149–2176.
- Donovan, J.J., Tingle, T.N., 1996. An improved mean atomic number background correction for quantitative microanalysis. *Microsc. Microanal.* 2 (1), 1–7.
- Donovan, J.J., Singer, J.W., Armstrong, J.T., 2016. A new EPMA method for fast trace element analysis in simple matrices. *Am. Mineral.* 101 (8), 1839–1853.
- Donovan, J., Kremser, D., Fournelle, J., Goemann, K., 2018. Probe for Windows user's Guide and Reference, enterprise edition. Probe Software, Inc., Eugene, OR.
- Ellis, B., Pimentel, A., Wolff, J.A., Etter, A., Cortes-Calderon, E.A., Harris, C., Mark, D.F., Neukampf, J., Bachmann, O., 2022. Geochemistry of the Pepom tephra deposits: the most recent intracaldera volcanism of Sete Cidades volcano, São Miguel, Azores. *J. Volcanol. Geotherm. Res.* 432, 107673.
- Farina, F., Dini, A., Innocenti, F., Rocchi, S., Westerman, D.S., 2010. Rapid incremental assembly of the Monte Capanne pluton (Elba Island, Tuscany) by downward stacking of magma sheets. *Geol. Soc. Am. Bull.* 122, 1463–1479.
- Farmer, G.L., Broxton, D.E., Warren, R.G., Pickthorn, W., 1991. Nd, Sr, and O isotopic variations in metaluminous ash-flow tuffs and related volcanic rocks at the Timber Mountain/Oasis Valley Caldera, complex, SW Nevada: Implications for the origin and evolution of large-volume silicic magma bodies. *Contrib. Mineral. Petrol.* 109, 53–68.
- Foley, M.L., Miller, C.F., Gualda, G.A.R., 2020. Architecture of a super-sized magma chamber and remobilization of its basal cumulate (Peach Spring Tuff, USA). *J. Petrol.* 61, 1, ega020.
- Forni, F., Bachmann, O., Mollo, S., De Astis, G., Gelman, S.E., Ellis, B.S., 2016. The origin of a zoned ignimbrite: insights into the Campanian Ignimbrite magma chamber (Campi Flegrei, Italy). *Earth Planet. Sci. Lett.* 449, 259–271.
- Freundt, A., Schmincke, H.-U., 1992. Mixing of rhyolite, trachyte and basalt magma erupted from a vertically and laterally zoned reservoir, composite flow p1, Gran Canaria. *Contrib. Mineral. Petrol.* 112 (1), 1–19.
- Freundt, A., Schmincke, H.-U., 1998. Emplacement of Ash Layers Related to High-Grade Ignimbrite P1 in the Sea around Gran Canaria. Texas A & M University.
- Freundt-Malecha, B., 2001. Plutonic rocks of intermediate composition on Gran Canaria: the missing link of the bimodal volcanic rock suite. *Contrib. Mineral. Petrol.* 141 (4), 430–445.
- Geist, D., Naumann, T., Larson, P., 1998. Evolution of Galapagos Magmas: Mantle and Crustal fractionation without assimilation. *J. Petrol.* 39, 953–971.
- Goldstein, J.I., Newbury, D.E., Echlin, P., Joy, D.C., Fiori, C., Lifshin, E., 1981. Practical techniques of X-ray analysis. In: *Scanning electron Microscopy and X-Ray Microanalysis*. Springer, Boston, MA, pp. 393–445.
- Guillong, M., Meier, D.L., Allan, M.M., Heinrich, C.A., Yardley, B.W., 2008. Appendix a6: Sills: A MATLAB-based program for the reduction of laser ablation icp-ms data of homogeneous materials and inclusions. *Mineral. Assoc. Can. Short Course* 40, 328–333.
- Gurenko, A.A., Chaussidon, M., Schmincke, H.-U., 2001. Magma ascent and contamination beneath one intraplate volcano: evidence from S and O isotopes in glass inclusions and their host clinopyroxenes from Miocene basaltic hyaloclastites southwest of Gran Canaria (Canary Islands). *Geochim. Cosmochim. Acta* 65 (23), 4359–4374.
- Gurenko, A.A., Hoernle, K., Hauff, F., Schmincke, H.-U., Han, D., Miura, Y., Kaneoka, I., 2006. Major, trace element and Nd–Sr–Pb–O–He–Ar isotope signatures of shield stage lavas from the central and western Canary Islands: Insights into mantle and crustal processes. *Chem. Geol.* 233 (1–2), 75–112.
- Gurenko, A.A., Bindeman, I.N., Chaussidon, M., 2011. Oxygen isotope heterogeneity of the mantle beneath the Canary Islands: Insights from olivine phenocrysts. *Contrib. Mineral. Petrol.* 162 (2), 349–363.
- Hamilton, D., MacKenzie, W., 1965. Phase-equilibrium studies in the system NaAlSi<sub>3</sub>O<sub>8</sub> (nepheline)–KAlSi<sub>3</sub>O<sub>8</sub> (kalsilite)–SiO<sub>2</sub>–H<sub>2</sub>O. *Mineral. Mag. J. Mineral. Soc.* 34 (268), 214–231.
- Hansteen, T.H., Troll, V.R., 2003. Oxygen isotope composition of xenoliths from the oceanic crust and volcanic edifice beneath Gran Canaria (Canary Islands): Consequences for crustal contamination of ascending magmas. *Chem. Geol.* 193 (3–4), 181–193.
- Harris, C., Vogeli, J., 2010. Oxygen isotope composition of garnet in the peninsula granite, cape granite suite, South Africa: Constraints on melting and emplacement mechanisms. *S. Afr. J. Geol.* 113 (4), 401–412.
- Harris, C., Marsh, J.S., Milner, S.C., 1999. Petrology of the alkaline core of the Messum igneous complex, Namibia: evidence for the progressively decreasing effect of crustal contamination. *J. Petrol.* 40 (9), 1377–1397.
- Higgins, M.D., 2011. Quantitative petrological evidence for the origin of k-feldspar megacrysts in dacites from Taapaca volcano, Chile. *Contrib. Mineral. Petrol.* 162 (4), 709–723.
- Hoernle, K., 1998. Geochemistry of jurassic oceanic crust beneath Gran Canaria (Canary Islands): Implications for crustal recycling and assimilation. *J. Petrol.* 39 (5), 859–880.
- Hoernle, K.A.J., Carracedo, J.C., 2009. *Canary Islands Geology*. University of California Press.
- Hoernle, K., Schmincke, H.-U., 1993. The role of partial melting in the 15-ma geochemical evolution of Gran Canaria: A blob model for the canary hotspot. *J. Petrol.* 34 (3), 599–626.
- Hoernle, K., Tilton, G., Schmincke, H.-U., 1991. SrNdPb isotopic evolution of Gran Canaria: evidence for shallow enriched mantle beneath the Canary Islands. *Earth Planet. Sci. Lett.* 106 (1–4), 44–63.
- Javoy, M., Stillman, C.J., Pineau, F., 1986. Oxygen and hydrogen isotope studies on the basal complexes of the Canary Islands: implications on the conditions of their genesis. *Contrib. Mineral. Petrol.* 92 (2), 225–235.
- Jochum, K.P., Weis, U., Stoll, B., Kuzmin, D., Yang, Q., Raczek, I., Enzweiler, J., 2011. Determination of reference values for NIST SRM 610–617 glasses following ISO guidelines. *Geostand. Geoanal. Res.* 35 (4), 397–429.
- Johnson, B.R., Glazner, A.F., 2010. Formation of k-feldspar megacrysts in granodioritic plutons by thermal cycling and late-stage textural coarsening. *Contrib. Mineral. Petrol.* 159 (5), 599–619.
- Landi, P., La Felice, S., Petrelli, M., Vezzoli, L.M., Principe, C., 2019. Deciphering textural and chemical zoning of K-feldspar megacrysts from Mt. Amiata Volcano (Southern Tuscany, Italy): Insights into the petrogenesis and abnormal crystal growth. *Lithos* 324–325, 569–583.
- Le Bas, M., Maitre, R.L., Streckeisen, A., Zanettin, B., on the Systematics of Igneous Rocks, I. S., 1986. A chemical classification of volcanic rocks based on the total alkali-silica diagram. *J. Petrol.* 27 (3), 745–750.
- McDougall, I., Schmincke, H.-U., 1976. Geochronology of Gran Canaria, Canary Islands: Age of shield building volcanism and other magmatic phases. *Bull. Volcanol.* 40 (1), 57–77.

- Metrich, N., Allard, P., Spilliaert, N., Andronico, D., Burton, M., 2004. 2001 flank eruption of the alkali- and volatile-rich primitive basalt responsible for Mount Etna's evolution in the last three decades. *Earth Planet. Sci. Lett.* 228, 1–17.
- Mills, R.D., Glazner, A.F., 2013. Experimental study on the effects of temperature cycling on coarsening of plagioclase and olivine in an alkali basalt. *Contrib. Mineral. Petrol.* 166, 97–111.
- Mills, R.D., Ratner, J.J., Glazner, A.F., 2011. Experimental evidence for crystal coarsening and fabric development during temperature cycling. *Geology* 39 (12), 1139–1142.
- Montelli, R., Nolet, G., Dahlen, F., Masters, G., 2006. A catalogue of deep mantle plumes: New results from finite-frequency tomography. *Geochem. Geophys. Geosyst.* 7 (11).
- Moussallam, Y., Oppenheimer, C., Scaillet, B., Buisman, I., Kimball, C., Dunbar, N., Burgisser, A., Schipper, A., Andujar, J., Kyle, P., 2015. Megacrystals track magma convection between reservoir and surface. *Earth Planet. Sci. Lett.* 413, 1–12.
- Pérez-Torrado, F.J., Carracedo, J.C., Mangas, J., 1995. Geochronology and stratigraphy of the Roque Nublo Cycle, Gran Canaria, Canary Islands. *J. Geol. Soc.* 152 (5), 807–818.
- Popa, R.G., Bachmann, O., Ellis, B.S., Degruyter, W., Tollan, P., Kyriakopoulos, K., 2019. A connection between magma chamber processes and eruptive styles revealed at Nisyros-Yali volcano (Greece). *J. Volcanol. Geotherm. Res.* 387, 106666.
- Popa, R.G., Bachmann, O., Huber, C., 2021. Explosive or effusive style of volcanic eruption determined by magma storage conditions. *Nat. Geosci.* 14 (10), 781–786.
- Raczek, I., Stoll, B., Hofmann, A.W., Peter Jochum, K., 2001. High-Precision Trace Element Data for the USGS Reference Materials BCR-1, BCR-2, BHVO-1, BHVO-2, AGV-1, AGV-2, DTS-1, DTS-2, GSP-1 and GSP-2 by ID-TIMS and MIC-SSMS. *Geostand. Newslett.* 25 (1), 77–86.
- Renne, P.R., Balco, G., Ludwig, K.R., Mundil, R., Min, K., 2011. Response to the comment by WH Schwarz et al. on “Joint determination of  $^{40}\text{K}$  decay constants and  $^{40}\text{Ar}^*/^{40}\text{K}$  for the fish Canyon sanidine standard, and improved accuracy for  $^{40}\text{Ar}/^{39}\text{Ar}$  geochronology” by PR Renne et al.(2010). *Geochim. Cosmochim. Acta* 75 (17), 5097–5100.
- Rodriguez-Gonzalez, A., Fernandez-Turiel, J.L., Perez-Torrado, F.J., Hansen, A., Aulinas, M., Carracedo, J.C., Paterne, M., 2009. The Holocene volcanic history of Gran Canaria island: implications for volcanic hazards. *J. Quat. Sci.* 24 (7), 697–709.
- Rout, S.S., Wörner, G., 2020. Constraints on the pre-eruptive magmatic history of the Quaternary Laacher See volcano (Germany). *Contrib. Mineral. Petrol.* 175, 73.
- Rout, S.S., Blum-Oeste, M., Wörner, G., 2021. Long-Term Temperature Cycling in a Shallow Magma Reservoir: Insights from Sanidine Megacrysts at Taápaca Volcano, Central Andes. *J. Petrol.* 62 (9), 1–32.
- Ruprecht, P., Wörner, G., 2007. Variable regimes in magma systems documented in plagioclase zoning patterns: El Misti stratovolcano and Andagua monogenetic cones (S. Peru). *J. Volcanol. Geotherm. Res.* 165, 142–162.
- Schipper, C.I., Castro, J.M., Tuffen, H., James, M.R., How, P., 2013. Shallow vent architecture during hybrid explosive–effusive activity at Cordón Caulle (Chile, 2011–12): evidence from direct observations and pyroclast textures. *J. Volcanol. Geotherm. Res.* 262, 25–37.
- Schirnack, C., van den Bogaard, P., Schmincke, H.-U., 1999. Cone sheet formation and intrusive growth of an oceanic island—the Miocene Tejeda complex on Gran Canaria (Canary Islands). *Geology* 27 (3), 207–210.
- Schmincke, H.-U., 1967. Cone sheet swarm, resurgence of Tejeda caldera, and the early geologic history of Gran Canaria. *Bull. Volcanol.* 31 (1), 153–162.
- Schmincke, H.-U., 1976. The geology of the Canary Islands. In: *Biogeography and Ecology in the Canary Islands*. Springer, pp. 67–184.
- Schmincke, H.-U., Sumita, M., 1998. 27. Volcanic evolution of Gran Canaria reconstructed from apron sediments: Synthesis of vicap project drilling1. *Proc. Ocean Drill. Prog.: Sci. Results* 157, 443–469.
- Sliwinski, J., Farsky, D., Lipman, P.W., Guillong, M., Bachmann, O., 2019. Rapid Magma Generation or Shared Magmatic Reservoir? Petrology and Geochronology of the Rat Creek and Nelson Mountain Tuffs, CO, USA. *Front. Earth Sci.* 7, 271.
- Spilliaert, N., Allard, P., Metrich, N., Sobolev, A.V., 2006. Melt inclusion record of the conditions of ascent, degassing, and extrusion of volatile-rich alkali basalt during the powerful 2002 flank eruption of Mount Etna (Italy). *J. Geophys. Res.* 111, B04203.
- Sumita, M., Schmincke, H.-U., 1998. Tephra event stratigraphy and emplacement of volcanoclastic sediments, Mogán and Fataga stratigraphic intervals, part i: Mineral and chemical stratigraphy of volcanoclastic units and correlation to the subaerial record. *Proc. Ocean Drill. Prog. Sci. Results* 157, 219–266.
- Sumner, J.M., Branney, M.J., 2002. The emplacement history of a remarkable heterogeneous, chemically zoned, rheomorphic and locally lava-like ignimbrite: “TL” on Gran Canaria. *J. Volcanol. Geotherm. Res.* 115 (1–2), 109–138.
- Sun, S.S., 1980. Lead isotopic study of young volcanic rocks from mid-ocean ridges, ocean islands and island arcs. *Philos. Trans. R. Soc. Lond. Ser. A, Math. Phys. Sci.* 297 (1431), 409–445.
- Szymanowski, D., Schoene, B., 2020. U–Pb ID-tIMS geochronology using ATONA amplifiers. *J. Anal. At. Spectrom.* 35 (6), 1207–1216.
- Szymanowski, D., Ellis, B.S., Bachmann, O., Guillong, M., Phillips, W.M., 2015. Bridging basalts and rhyolites in the Yellowstone–Snake River Plain volcanic province: The elusive intermediate step. *Earth Planet. Sci. Lett.* 415, 80–89.
- Szymanowski, D., Wotzlaw, J.F., Ellis, B.S., Bachmann, O., Guillong, M., von Quadt, A., 2017. Protracted near-solidus storage and pre-eruptive rejuvenation of large magma reservoirs. *Nat. Geosci.* 10, 777–782.
- Thirlwall, M., Jenkins, C., Vroon, P., Matthey, D., 1997. Crustal interaction during construction of ocean islands: Pb, Sr, Nd, O isotope geochemistry of the shield basalts of Gran Canaria, Canary Islands. *Chem. Geol.* 135 (3–4), 233–262.
- Troch, J., Ellis, B.S., Harris, C., Ulmer, P., Bachmann, O., 2018. The effect of prior hydrothermal alteration on the melting behaviour during rhyolite formation in Yellowstone, and its importance in the generation of low- $\delta^{18}\text{O}$  magmas. *Earth Planet. Sci. Lett.* 481, 338–349.
- Troll, V.R., Schmincke, H.-U., 2002. Magma mixing and crustal recycling recorded in ternary feldspar from compositionally zoned peralkaline ignimbrite ‘A’, Gran Canaria, Canary Islands. *J. Petrol.* 43 (2), 243–270.
- Tuffen, H., Dingwell, D.B., Pinkerton, H., 2003. Repeated fracture and healing of silicic magma generate flow banding and earthquakes? *Geology* 31 (12), 1089–1092.
- Tuttle, O.F., Bowen, N.L., 1958. Origin of Granite in the Light of Experimental Studies in the System NaAlSi<sub>3</sub>O<sub>8</sub>-KAlSi<sub>3</sub>O<sub>8</sub>-SiO<sub>2</sub>-H<sub>2</sub>O, vol. 74. Geological Society of America. *Ocean Drill. Prog.: Sci. Results* 157 (Chapter 11), 127–140.
- Wadsworth, F.B., Llewellyn, E.W., Vasseur, J., Gardner, J.E., Tuffen, H., 2020. Explosive-effusive volcanic eruption transitions caused by sintering. *Sci. Adv.* 6 (39) eaba7940.
- Wieser, P.E., Edmonds, M., Gansecki, C., MacLennan, J., Jenner, F.E., Kunz, B., Antoshchikina, P., Trusdell, F., Lee, R.L., 2022. Explosive activity on Kilauēa’s lower East Rift Zone Fueled by a Volatile-Rich, Dacitic Melt. *Geochem. Geophys. Geosyst.* 23 e2021GC010046.
- Wilson, J.T., 1963. A possible origin of the Hawaiian Islands. *Can. J. Phys.* 41 (6), 863–870.
- Wolff, J.A., 1987. Crystallisation of nepheline syenite in a subvolcanic magma system: Tenerife, Canary Islands. *Lithos* 20 (3), 207–223.
- Wolff, J.A., 2017. On the syenite-trachyte problem. *Geology* 45 (12), 1067–1070.
- Wolff, J.A., Grandy, J., Larson, P., 2000. Interaction of mantle-derived magma with island crust? Trace element and oxygen isotope data from the diego hernandez formation, las canadas, Tenerife. *Journal of Volcanology and Geothermal Research*, 103(1–4), 343–366. Zindler, A., Hart, S.R. (1986). Chemical geodynamics. *Annu. Rev. Earth Planet. Sci.* 14, 493–571.
- Wolff, J.A., Ellis, B.S., Ramos, F.C., Starkel, W.A., Borroughs, S., Olin, P.H., Bachmann, O., 2015. Remelting of cumulates as a process for producing chemical zoning in silicic tuffs: A comparison of cool, wet and hot, dry rhyolitic magma systems. *Lithos* 236–7, 275–286.
- Wolff, J.A., Forni, F., Ellis, B.S., Szymanowski, D., 2020. Europium and barium enrichments in compositionally zoned felsic tuffs: A smoking gun for the origin of chemical and physical gradients by cumulate melting. *Earth Planet. Sci. Lett.* 540, 116251.
- Zindler, A., Hart, S.R., 1986. Chemical geodynamics. *Annu. Rev. Earth Planet. Sci.* 14, 493–571.